Clarkson University

Spectral and Photometric Analysis of the Binary Hypergiant R81 in the Large Magellanic Cloud

A Thesis By

Benjamin R. Roulston

Department of Physics

Submitted in partial fulfillment of the requirements for a

Bachelor of Science with University Honors

April 2016

Accepted by the Honors Program

Joshua D. Thomas 4/27/2016

Advisor (Dr. Joshua D. Thomas) Date

Jan Scrimgeour 4/29/2016

Honors Reader (Dr. Jan Scrimgeour) Date

_____

Honors Director (Dr. Jon Goss) Date

ABSTRACT

This work studies the eclipsing binary system R81 in the Large Magellanic Cloud. From the spectroscopic and photometric data, various details about the R81 system were determined. The photometric data allowed for the determination of a more accurate period (74.554 days) for this system. The photometric measurements were then phase folded and plotted to show the light curve and eclipse of the system. The spectroscopic data were measured for radial velocities and phase dependences on equivalent widths and emission/absorption intensity. Using all 21 spectra, a dynamical spectrum was made for the Hα line. This dynamical spectrum showed an increase in emission at two phases of the orbit. This emission increase is a key indicator of what we believe to be some form of mass transfer between the primary and secondary stars. This emission and mass transfer is the focus of the ongoing research.

ACKNOWLEDGMENTS

I would like to first thank my advisor Dr. Joshua Thomas. Without him, I would never have had the amazing opportunities that I have experienced over the last 2 years. He has been a constant mentor and friend throughout the entire project, and I definitely would not have been able to make it this far without him.

I also want to thank Dr. Noel Richardson for his help with this project. I would not have had any spectra on this object and the outcomes of this project would have been severely limited without his support and collaboration. Noel has been a great source of information and guidance when an outside opinion on the data analysis was needed.

Lastly, I want to thank Katelyn Legacy for her constant support through all of my research. Without her, I would still be procrastinating most of my work and this thesis would still probably be half written. Thank you for your constant push, and for your constant proofreading of my work. It is deeply appreciated.

Contents

List of Tables

List of Figures

Chapter 1

Introduction

While many people may look at the night sky and admire the stars, most are blind to the true beauty of these objects. The light that left these objects thousands of years ago (if not *millions* for some) falls onto our telescopes and detectors, containing more information than just what the object looked like at that time. By using advanced computational methods, it is possible to use this starlight to determine the hidden information contained within. A few brief examples related to this work include photometry and spectroscopy. Photometry can be used to measure the variations in luminosity of an object over time to determine if there are intrinsic pulsations or maybe a transit of some unknown object. Spectroscopy can be used to determine the chemical composition of the object and the environment surrounding the object in which the light comes from, as well as anything along the line of sight. In addition to recent advances in computing power, it is now possible to run large scale simulations of events such as the formation of the Universe after the Big Bang or the merging of two galaxies. These are just a few representative examples of the many things possible today in the different research subfields of astronomy and astrophysics.

This project investigated the binary system RMC-81 (R81) in the Large Magellanic Cloud. R81 is an transiting eclipsing binary star system, consisting of a possible luminous blue variable (LBV) supernova precursor. R81 was originally studied in-depth by Tubbesing et al. (2001) who later followed up their previous work with Tubbesing et al. (2002). In this project, we used data obtained from spectroscopic and photometric measurements with the goal being to find evidence for mass transfer between the binary stars. The majority of this project involved studying and analyzing approximately 30 years worth of photometric measurements and a substantial orbital phase sampling of spectroscopic data. The results from this analysis was used to infer the physical conditions of the binary stars. From this, different physical processes were examined to evaluate which ones were the most plausible to create the features observed in the data sets.

Chapter 2

Literature Review

2.1 Binary Stars

The majority of "stars" in the sky are actually systems of two or more stars. These systems, called binary systems, are actually as common as individual stars as shown by Abt (1983). In a binary star system, two stars orbit around their common center of mass. It is possible to have more than two stars in a system, there are cases such as α Gem which is a system totaling 6 stars. This research focused on R81 which is a transiting eclipsing binary system. Due to the high number of observable binary systems, there are a wide range different physical situations that can be found while studying binary stars.

In a binary system there are certain physical parameters that need be known in order to understand and describe the system. The main parameters that describe the binary orbit itself can be seen in Table 2.1. This table does not include all orbit parameters, but the ones that are of most importance as well as most likely to be found and discussed in studying the behavior of binary orbits.

Table 2.1 Important Binary System Parameters

Parameter	Unit	Description
P	days	period of the binary orbit
e	—	eccentricity of the orbit
i	$\circ$	inclination angle of orbit
M	$M_\odot$[1]	mass of star
q	—	mass ratio of stars $\left(\frac{M_1}{M_2}\right)$
V_r	km s^{-1}	radial velocity of star

[1] $M_\odot$ is the solar mass

2.2 Interacting Binary Stars

While there are many different configurations of binary systems, they all can be placed into five general classifications. These classifications are based on the Roche lobes of the two stars. The Roche lobe is an imaginary shell surrounding a star. This "shell" is the representation of the extent of the gravitational hold on the mass of the star. That is, anything within the Roche lobe is gravitationally bound to the star, while anything on the outside of this shell is not bound and can be lost into space or transfered to the other star (Hilditch, 2001).

The Roche lobe can be visualized by creating a plot of the gravitational equipotential lines around a binary system. Gravitational equipotential lines are lines which follow a constant gravitational field. That is, the gravitational force along a equipotential line is the same everywhere on that line. The points where the two gravitational forces of the stars balance out are called the Lagrange points, all of which are in the orbital plane. The point where the two Roche lobes of the stars meet is known as the "inner" Lagrange point, the $L1$ point. An example of these gravitational equipotential lines are shown in Figure 2.1 for the four different types of close binary systems.

Figure 2.1.a illustrates a *detached* binary. A detached binary is one in which the surface of both stars are within their respective Roche lobes. Since both of the stars are within their respective Roche Lobes, material is bound to each star, and this type of binary will not have mass loss or transfer.

Figure 2.1.b shows a *semi-detached* binary. A semi-detached binary is binary where one of the stars fills, or even overfills, its Roche lobe, while the other star is still within its Roche lobe. In this type of binary system, the star that fills its Roche lobe may lose material and mass through the $L1$ to its companion star or off the star into space. This material may also form an accretion disk around the companion star.

Figure 2.1.c shows a *contact* binary. In a contact binary, both stars fill or overfill their Roche

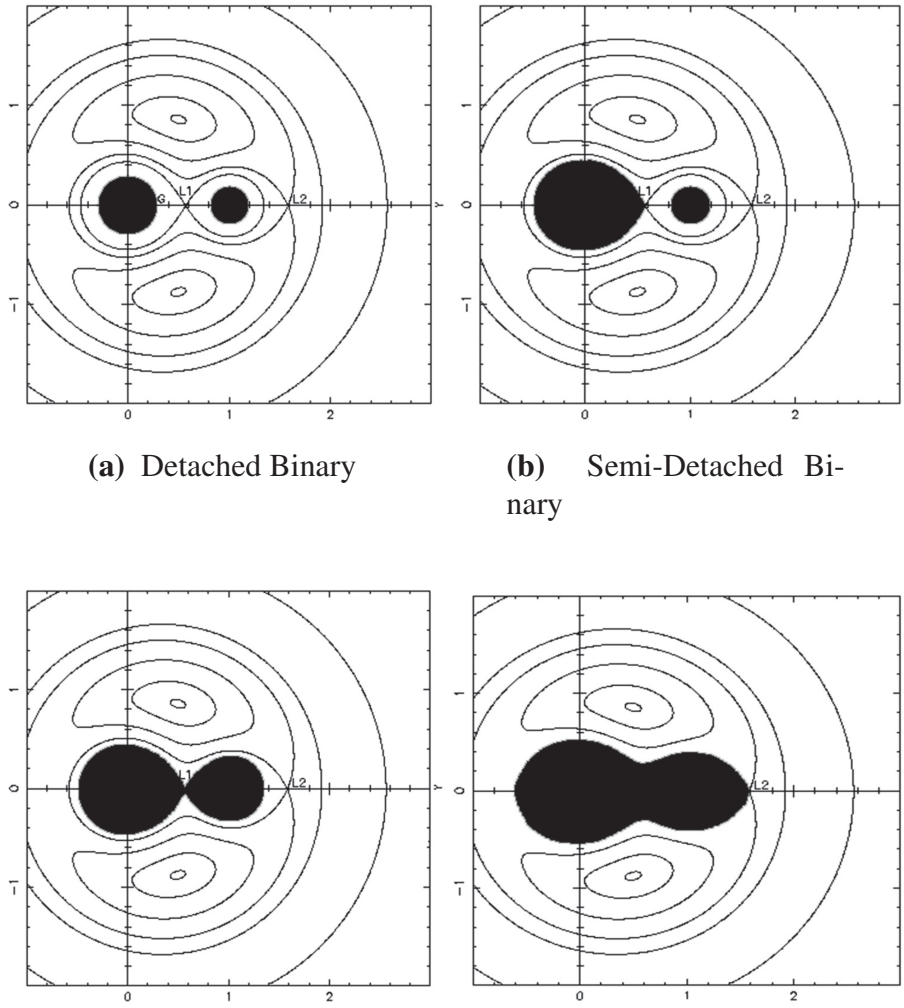

(a) Detached Binary

(b) Semi-Detached Binary

(c) Contact Binary

(d) Common Envelope (Overcontact) Binary

Figure 2.1 Gravitational equipotential plots for four different types of binary systems. Plots from Professor Vik Dhillon at the University of Sheffield (Dhillon, 2008).

lobes and their "surfaces" are in contact. Mass may be transfered from the more massive to the less massive star through the $L1$. In this case, the stars atmospheres may begin to interact due to the contact between them and different physical effects can be seen.

Figure 2.1.d is the last type of binary type and is called a *common envelope* binary, also known as an *overcontact* binary. In an overcontact binary, both stars overfill their Roche lobes. The stars share a common atmosphere, and they interact greatly in their lives together. The rotation about their center of mass while being in such close contact creates enormous friction, heating up the shared part of the atmosphere, and causes the system to lose rotational energy. This can allow for the degradation of the orbit and can even lead to a merger of the two stars ending in a possible supernova.

Depending on the classification scheme, there maybe a fifth type of binary, the *cataclysmic variable*. This is where a normal main sequence star fills its Roche lobe and has a compact companion. The compact companion can be a white dwarf, a neutron star, or even a black hole. This type was not included in the plots due to the difficulties of representing the intense gravitational field surrounding a compact object.

2.3 Photometry

The second method that was used for this work is photometry. Photometry is the measurement of the brightness, flux, and magnitude of a star or stars. Stars are classified by their magnitude which is a measure of their flux or luminosity. The magnitude scale is a logarithmic one due to its founding on the human eye which reacts logarithmically to light. Magnitudes are always in relation to another object and are given by Equation 2.1.

$$m_1 - m_2 = -2.5 \log_{10} \left(\frac{f_1}{f_2} \right) \tag{2.1}$$

In Equation 2.1, m_1 and m_2 are the magnitudes of the two objects and f_1 and f_2 are the fluxes of the two objects. Alternatively, the fluxes can be replaced with E_1 and E_2 which are the energy per unit area on Earth from the two objects. From this equation, it is seen that an object with a larger brightness will have a smaller magnitude while a fainter object will have a larger magnitude.

From this equation, it is possible to find the magnitude of any object relative to another object. In order to compare magnitudes, a system of standard stars is used to find a stars "absolute" magnitude. This standard (or reference) star is a photometric standard in which the magnitude is defined to be a certain value and all other magnitudes are based off that star.

One of the many useful purposes of photometry is to monitor changes and variations in the magnitude of a star. Small periodic variations may be a clue for stellar pulsations or a partial eclipse. These partial eclipses could be cause by transiting exoplanets, and photometry is the main method of detection of these. While large, deep changes in magnitude are a good sign of some type of binary eclipse. By tracking these eclipses, it is possible to determine periods from the data and then use that period to calculate the orbit parameters.

2.4 Spectroscopy

Spectroscopic analysis was one of the focuses of this project. There are many processes that must be understood in order to understand how spectroscopy works and how to get the information we need out of it. The first part of spectroscopy is how light and matter interact. Matter is made of discrete objects called atoms. These atoms consist of an electrically positive nucleus surrounded by a negatively charged electron "cloud". Each of these electrons occupy a space around the nucleus, depending on the electron's energy, called an energy level. Each neutral an ionized atom has a different number of electrons and thus has a different number of orbitals filled. Each orbital has a different configuration depending on the number of electrons in the atom or molecules. It is these

electrons in their energy levels that light will interact with.

Light can be thought of as either a particle or a wave. In the particle notation, light is made of discrete quantized packets called photons. Depending on the wavelength of light, these photons will have varying amounts of energy.

If the energy of a photon exactly matches that of an energy level of an electron in the atom that electron can use the energy from the photon to change energy levels, exciting the electron, which in turn absorbs the photon. The opposite can also occur; starting with an excited electron can transition down energy levels in specific steps determined by the quantum numbers with each transition emitting a photon with energy equal to that of the transition energy. As the electron transitions down the energy levels, it can go through different combinations of energy levels. This allows for an electron to be excited by one photon of a certain energy; then that electron transitions back down releasing, for example, three new photons of different energies.

It is this process of absorption and emission that creates the spectral lines found when light is broken up with a spectrograph. The absorption and emission lines are caused by the transitions of electrons in atoms. The atoms that produce the lines do not have to be from the source, only between the source and the observer. This is described in Kirchhoff's Laws given by Gustav Kirchhoff in 1860 (Carroll and Ostile, 2007).

1. A hot, dense gas or solid object produces a continuous spectrum with no dark spectral lines

2. A hot, diffuse gas produces bright spectral lines

3. A cool, diffuse gas in front of a source of continuous spectrum produces dark spectral lines in the continuous spectrum

Therefore, the lines in the spectra we see may be from the star, an envelope around the star, or interstellar medium between the object and the observer (Emerson, 1996). However, if the tem-

perature of the material is the same as the background it will not be possible to observe spectral features.

The next process in spectroscopy takes advantage of the wave property of light. The light that is to be studied is directed onto a diffraction grating. This diffraction grating is usually glass with thousands of grooves per millimeter engraved onto the surface. These grooves act like thousands of double slits, which cause the light to diffract (Fowles, 1989). It is through this diffraction process that the true information in the light can be seen. As with any wave when light diffracts, the amount by which it diffracts is wavelength dependent. Since light is a continuous spectrum of a number of different wavelengths, the light will be spread out into all the different wavelengths it is made of. This allows for the emission and absorption lines in the light to be detected and recorded for analysis later.

Once the spectrum has been recorded, there are two different methods of examining the spectrum. The first, called first order spectroscopy, examines the specific wavelengths of the lines that are formed. The individual lines are examined for their wavelength which gives insight into the chemical composition of the source. This is the method that is used to find the composition of stars, the interstellar medium, and nebulae. The second method is called second order spectroscopy and involves examining the structure and features of the spectral lines. This includes the shape, broadening, wings, equivalent widths (EQW) of the lines, and any other line feature. These features all give detail into the process and environments in which the lines were formed. Some examples of these line features from this work include varying EQW, or P-Cygni profiles (described in Section 2.5).

2.5 R81

The star R81 (Feast, Thackeray, & Wesselink, 1960) is an extremely bright B supergiant located in the Large Magellanic Cloud (LMC) that is a satellite galaxy to our own Milky Way (Tubbesing et al., 2002). The known binary parameters for R81 can be found in Table 2.2. Appenzeller (1972) showed that R81 exhibited an unusually high light variation of about 0.4 magnitudes. A light variation of this size was unusual for this spectral type and suggested a binary companion to the primary R81 (Tubbesing et al., 2001). It is believed that the primary star is a luminous blue variable (LBV or S Doradus variable) and a supernove precursor. LBVs are massive evolved stars that are characterized by photometric and spectroscopic variations as well as outbursts (Carroll and Ostile, 2007). The stars are unstable and can have periods of dramatic brightness increase and high mass loss through eruptions and ejections. The more prominent features of the R81 system include strong hydrogen lines in the Balmer and Paschen series as well as strong P-Cygni profile in the spectral lines (Tubbesing et al., 2002). R81 was also suspected to have a high mass loss rate through its wind which was found to be $\dot{M} = 3 \times 10^{-5} M_{\odot} yr^{-1}$ by Wolf et al. (1981).

R81 has a shell of material from the star's wind blowing out into space around the star (Tubbesing et al., 2001). This is known because of the P-Cygni profile we find in the spectrum of R81. This unique spectral feature is characteristic of an envelope of material surrounding a star with high mass loss such as those found in LBVs. As the star loses mass through its wind, the radiation pressure pushes the material away from the star into an expanding envelope surrounding the star. The gas directly in front of the star in our line of sight behaves according to (iii) of Kirchoff's Laws and absorbs the light from the star, creating absorption lines. This gas is expanding towards us, resulting in a Doppler shift, causing the gas in front of the star to make a blue-shifted absorption line. The gas on the edge of the star absorbs the light and re-radiates it, creating red-shifted emission lines. When the light from the star is studied, we see a superposition of all these features,

Table 2.2 R81 System Parameters

Parameter	Unit	Value
P	days	74.566 ± 0.014
e	—	0.569 ± 0.031
T_{eff}	K	19500 ± 2000
R	$R_{\odot}$	96
m_U	mag	9.77
m_B	mag	10.52
m_V	mag	10.52
m_R	mag	10.29
m_I	mag	10.29

creating the P-Cygni profile. A diagram explaining this process can be seen in Figure 2.2.a. The spectrum of R81 in Figure 2.2.b clearly shows this feature. The blue-shifted absorption can be seen on the left of the Hα line and the red-shifted emission can be seen on the right. This line shape is characteristic to stars with an envelope of material surrounding the star.

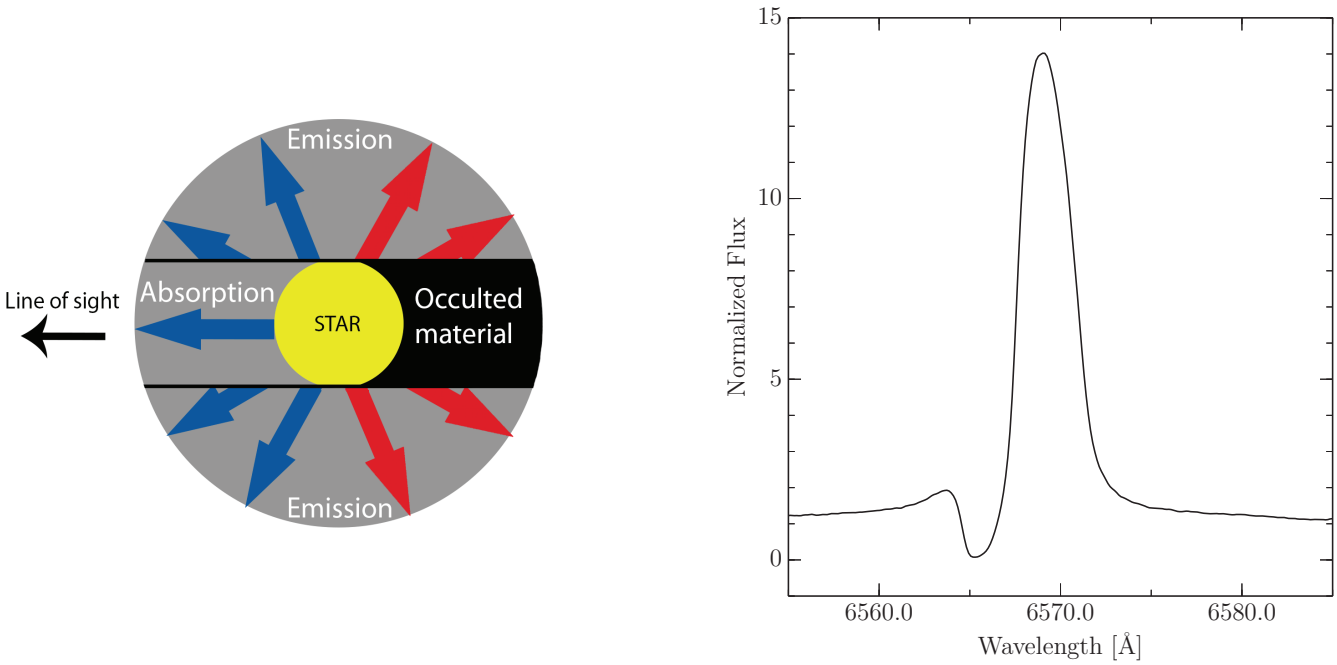

(a) Diagram of physical explanation of P-Cygni profile. The color of the arrow represents the Doppler shift of the material.

(b) P-Cygni profile of the Hα line in the spectrum of R81.

Figure 2.2 Diagram and sample P-Cygni profile for R81

Chapter 3

Data and Analysis

3.1 Data Acquisition

3.1.1 Spectroscopic

For the spectroscopic analysis, this research used 21 spectra of R81 obtained from the Cerro Tololo Inter-American Observatory (CTIO) in Chile. The spectral wavelengths range from ≈ 4500 — 8900Å with some discontinuities near the ends of the spectrum from the reduction of the raw spectra. The spectra were taken on the CTIO 1.5m telescope operated by the SMARTS Consortium with a cross-dispersed echelle spectrograph. The resolving power of the spectrograph is $R \approx 30\,000$. The resolving power is given by Equation 3.1. The higher the resolving power, the more features you will be able to see, and the more accurate velocity measurements you will have.

$$R = \frac{\lambda}{\Delta\lambda} = \frac{c}{\Delta v} \tag{3.1}$$

The spectra were collected between HJD2455993.6—HJD2456593.9, where HJD is the Heliocentric Julian Day. The HJD is a time system which counts the full number of days since some zero-point with the reference point of the Sun. This allows for standard time keeping and tracking of observations around the world.

3.1.2 Photometric

The data in the photometric analysis was collected from three different sources. The first set was obtained from Tubbesing et al. (2002). This data set included 86 points between HJD2451111.8—HJD2451211.6. The second data set was obtained from the Long-Term Photometry of Variables (LTPV). LTPV is a program run by the European Space Observatory (ESO). This data set included 41 data points between HJD2448166.7—HJD2448659.617. The last, and largest, data set was

obtained from the All Sky Automated Survey (ASAS). The ASAS data contains 664 data points obtained from HJD2451877.7—HJD2455157.7.

All of the data used in the photometric analysis can be found online from the CDS portal. The photometric data is not included in a table in this paper due to the large number of data points which totaled over 900.

3.2 Reduction

3.2.1 Spectroscopy

The spectra were corrected for the heliocentric (rest frame of the Sun) velocity of the Earth around the sun using the standard procedure in *Image Reduction and Analysis Facility* (IRAF). IRAF is the standard for data analysis of astronomical data. This correction allowed us to measure the radial velocity of R81 without the period of Earth orbiting the sun interfering with the measurements since these artifacts can leave traces in the radial velocity light curves.

After the spectra were corrected for heliocentric velocities, they were ready to be measured. From the spectra, we measured the velocities of the material certain spectral lines were formed in. We used the Doppler shift to measure the velocity of a spectral line.

The Doppler shift is a property of waves which describes how a moving source of a wave changes the wavelength of the wave. If the source is moving away from the observer, the wavelength appears to the observer to increase or shift to the “red” end of the spectrum. If the source is moving toward the observer the wavelength appears to the observer to be shorter or shift to the “blue” end of the spectrum. This process can be described by Equation 3.2, for the approximation when $v \ll c$. In this equation λ_0 is the rest wavelength of the light, $\lambda_{obs.}$ is the observed or measured

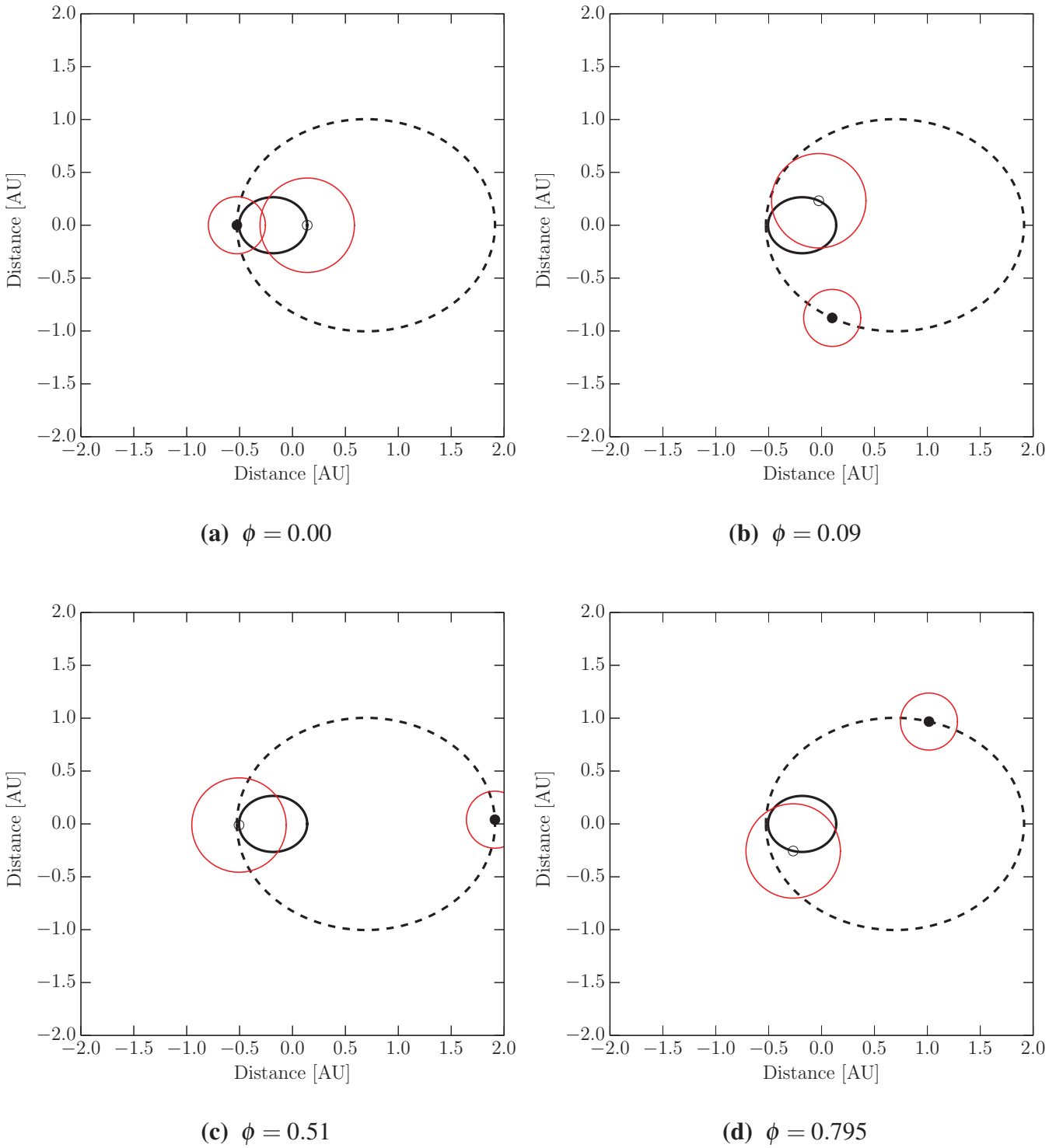

(a) $\phi = 0.00$

(b) $\phi = 0.09$

(c) $\phi = 0.51$

(d) $\phi = 0.795$

Figure 3.1 Important phases of R81's orbit. The observer is at the bottom left corner. These plots were created using the orbital parameters from Tubbesing et al. (2002). The red circles are the radii of the stars from Tubbesing et al. (2002). The larger star in the solid orbit is the primary star, while the smaller star in the dashed orbit is the secondary star.

wavelength, c is the speed of light, and v_s is the velocity of the source.

$$v_s \approx \left(\frac{\lambda_{obs.} - \lambda_0}{\lambda_0} \right) c \tag{3.2}$$

IRAF is used to measure the wavelength at which the lines appear to be at. This is done by fitting a Gaussian profile to the emission or absorption line and finding the line center in order to get $\lambda_{obs.}$. Depending on the velocity of the material, two lines may be blended together. Blending of lines is when two spectral lines intersect. This causes some problems when trying to determine whether the emission/absorption is coming from one line or the other. If two lines are blended together, IRAF has a deblending tool that allows the fit of multiple Gaussian profiles to each blended line in order ensure accurate measurements from the correct lines. Once the line centers are measured, we can use Equation 3.2 to find the velocity of either the star, the star's wind, or the shell surrounding the star. Table 3.1 gives the measured wavelength and radial velocity of a number of lines of R81. These velocities are averaged from measurements of all 21 spectra.

Figure 3.2 shows the radial velocity of SiIII line at $\lambda = 4552.6$Åwhich is one of the atmospheric lines of R81. This line was the one that provided the highest signal to noise ratio. This atmospheric line is formed only in the atmosphere of the star which allows us to determine the velocity of the star itself separately from the wind of material around the star. From this plot we can see the velocity at which the system is moving toward or away from us. The average velocity is $v_r \approx 175$ km s^{-1} away from us.

While measuring the line centers for velocities, we also looked at line shape and equivalent widths (EQW). The shape, or profile, of a line can provide details about the environment it was formed in or any unusual processes that may have aided in its formation. EQW is defined as the width of a box that comes from continuum to the peak of the line and has the same area as the area under the spectral line (Carroll and Ostile, 2007). It is given by Equation 3.3, where F_c is the flux

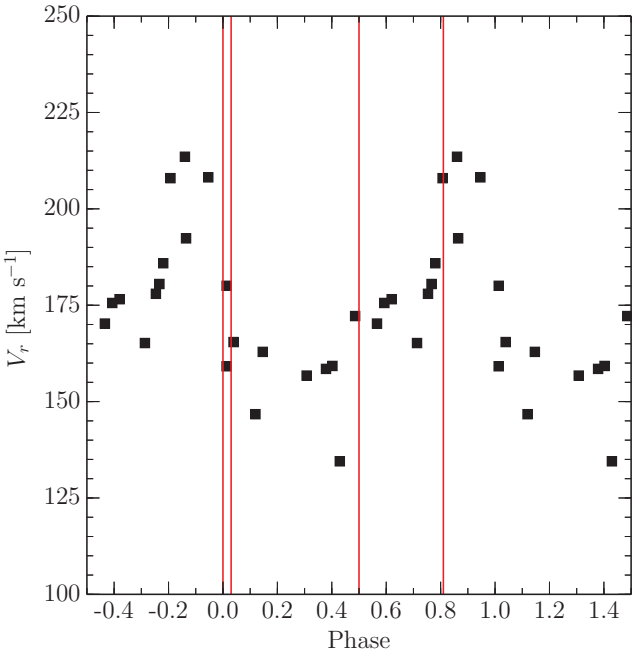

Figure 3.2 Radial velocity of the SiIII line at $\lambda = 4552.62$Å. Red lines are marked for the important phases of: $\phi = \{0.0, 0.08, 0.5, 0.8\}$.

at continuum and F_λ is the line flux.

$$EQW = \int \frac{F_c - F_\lambda}{F_c} d\lambda \tag{3.3}$$

IRAF has a function to automatically find the EQW of a line using the Gaussian profile. It also has a dedicated tool to measure EQW. Both of these methods were used in measuring the lines for this research.

3.2.2 Photometry

For the photometric data, there was not much left to do in the reduction process. Tubbesing et al. (2002), LTPV, and ASAS data are already reduced and available from online databases. For this research, we required measurements of high quality and accuracy and therefor only ASAS data of grade "A" was kept. The data from the LTPV program and from Tubbesing et al. (2002) have

Table 3.1 Radial Velocity Measurements

Line	λ [Å]	$\lambda_{obs.}$ [Å]	V_r [km s^{-1}]
HeI	4713.15	4717.06	251
	4921.93	4925.95	246
	5015.68	5019.60	235
	5875.62	5879.71	209
	6678.15	6683.00	218
	7065.19	7070.40	220
AlIII	5696.60	5701.27	198
SiII	5957.56	5962.68	217
	5978.93	5983.92	212
SiIII	4552.62	4556.72	176
	4567.82	4571.80	169
	4574.76	4579.00	181
	5739.73	5744.79	214

already been reduced and were considered of high quality since they have been published.

Chapter 4

Analysis and Results

4.1 Photometry

For the photometric analysis, we wanted to find a more accurate period for the binary. For this, all the photometric data were combined into one master set of measurements. This set contained the HJD of the observation and the V magnitude of R81. The V magnitude is the magnitude in the V filter of the Johnson filter system corresponding the effective wavelength midpoint of $\lambda_{\text{eff.}} = 551$nm with a full width half maximum of $\Delta\lambda = 88$nm. This set of all measurements was analyzed using Period04, a program designed to fit a period to unevenly spaced periodic data. The period fitting is done using a Lomb-Scargle periodogram. The period found for each of the data sets, along with the error, can be found in Table 4.1. In the same table the period for all photometric data combined can also be found which gave the most accurate period of the binary. The large errors (δP) found on the Tubbesing et al. (2002) and LTPV data sets are due to the small number of measurements in these data samples. In order for the periodogram to obtain better results, large data sets are required which explains why the error for the ASAS data is so much smaller. The ASAS data contained over 700 points alone. To get the best period for the binary, all photometric data was combined to get a data set of over 900 points. This allowed us to get a period with an error of approximately $\delta P = 56.16$ minutes.

Table 4.1 Photometric Period Fitting Results

Data Set	P [days]	$\pm\delta P$ [days]
Tubbesing et al. (2002)	71.9338	3.690
ASAS	74.6485	0.069
LTPV	74.8097	4.641
ALL COMBINED	74.5541	0.039

The data from all photometric measurements can been seen in Figure 4.1.a. This data has been phase folded with the period found from the analysis in this paper. Phase folding is the process in which you turn the date (HJD) of an observation into the phase of the orbit (where it is in the orbit), with reference to some "time zero" (T_0). For these plots, T_0 is the photometric minimum found by Tubbesing et al. (2002) which is $T_0 = 2451193.1$ in HJD. To find the phase at a time, you use Equation 4.1.

$$\phi = \frac{HJD - T_0}{P} \tag{4.1}$$

Equation 4.1 gives you ϕ which is the phase of the orbit at the time input and is a number greater than zero. The integer part of this number is the number of eclipses that have passed since T_0 and the decimal portion is how much of the orbit has been completed so far. Since we only care about where the stars are in the orbit and not how many times they have gone around (at least for our research), we take Mod 1 of the phase to get the real phase of how much of the orbit has been completed since T_0.

From Figure 4.1.a we can see the periodic motion of the light curve. However, there is a large scatter in the light curve; to get a better idea of what is going on with the system, we phase binned all the photometric data. Phase binning is the process of creating an average light curve from a large set of data. We phase binned our data into 50 bins. To do this, we made 50 bins between $\phi = 0.0$ and $\phi = 1.0$. Any phase that was in each phase range was averaged with all the others in that range (bin) and a standard deviation was calculated. The phase binned data can be seen in Figure 4.1.b.

In this phase binned plot, it is easy to see the periodic motion of the light curve. The most notable feature is the primary eclipse at phase $\phi = 0.0$. This is from the secondary star passing in front of the primary star. The eclipse seems to be ≈ 0.5 mag deep. There also seems to be a secondary periodic variation on top of the eclipse. This periodic variation seems to be triangular in shape and could be from a reflection in the system, some other geometric alignment in the binary

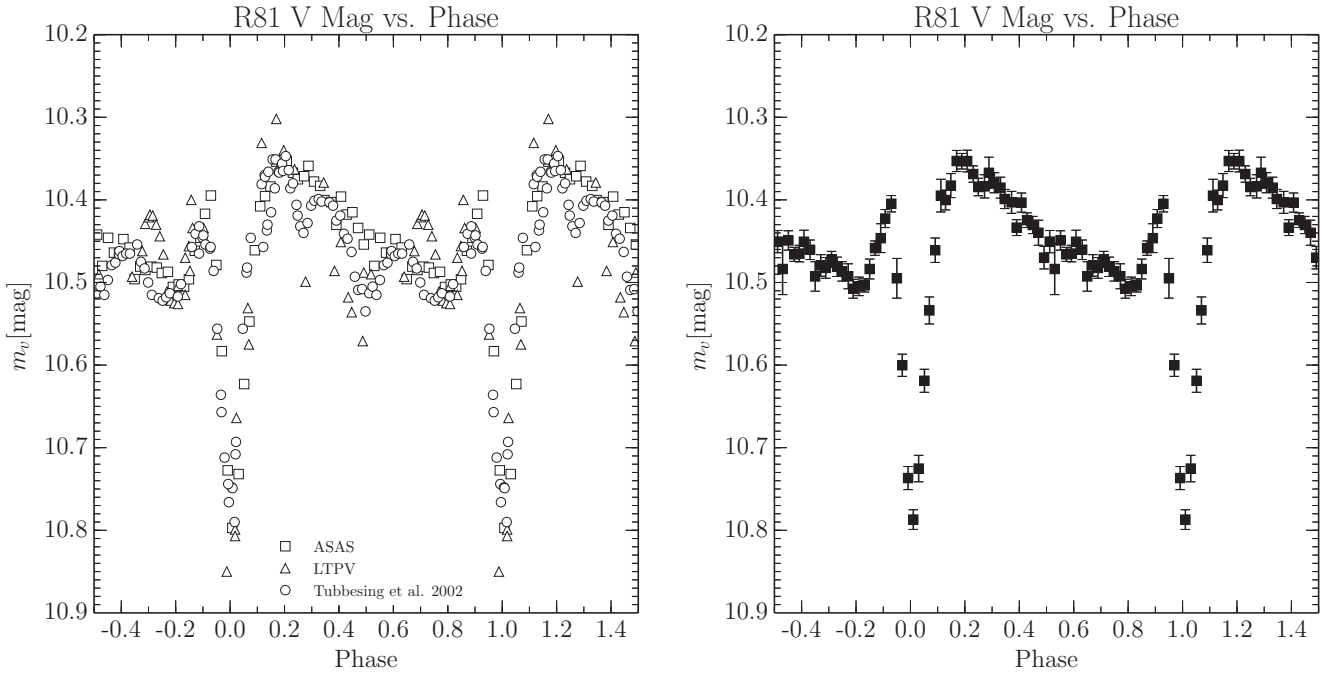

(a) All Photometric Raw **(b)** All Photometric Phase-Binned

Figure 4.1 All photometric data phase folded with calculated period. Both all raw measurements and phase binned data.

system, or an intrinsic variability in the light output of the stars. Tubbesing et al. (2002) believed there was a secondary eclipse around phase $\phi = 0.8$ which we do not see in our phase binned light curve.

4.2 Spectroscopy

For the spectroscopic data, there were a range of different measurements done. To measure the radial velocity of the star at the different phases of its orbit, 13 different lines from 3 different elements were measured for the doppler shift in the core of the line. These measurements, as well as the corresponding radial velocities, are found in Table 3.1. From these lines, it was hard to notice an orbital phase dependence which may be due to the low signal to noise ratio of the spectra.

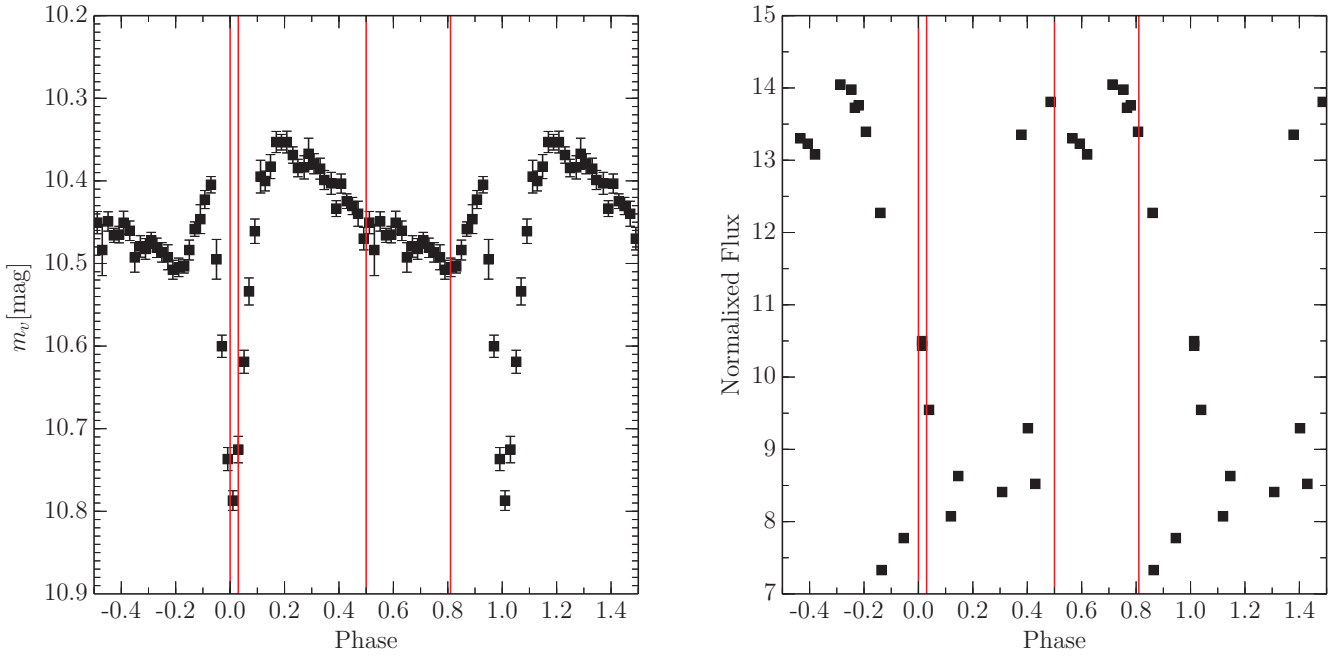

(a) Phase-binned photometric V magnitude

(b) Normalized flux of R81 Hα emission

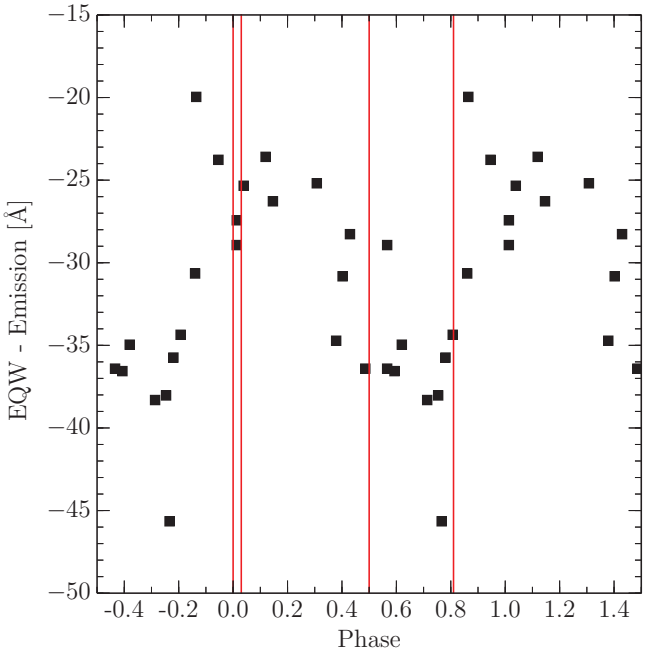

(c) EQW of R81 Hα emission

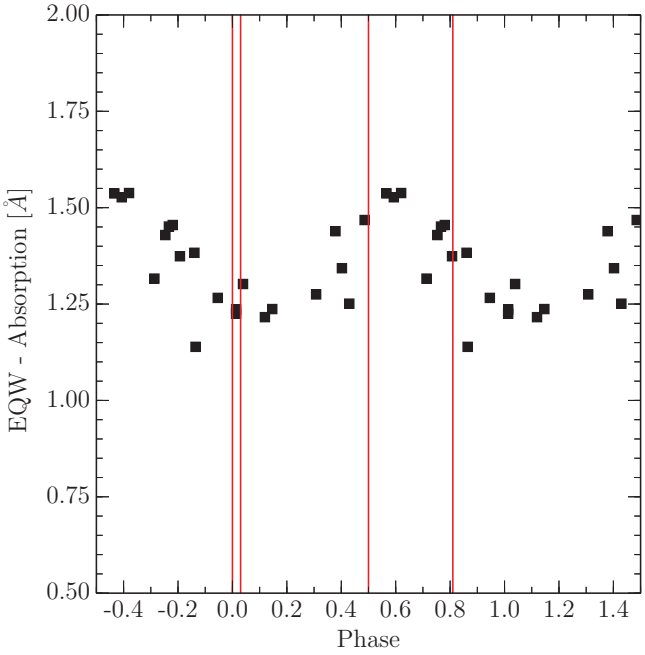

(d) EQW of R81 Hα absorption

Figure 4.2 Important plots of R81 data. Red lines are marked at the important phases of R81's orbit: $\phi = \{0.0, 0.08, 0.5, 0.8\}$. These phases are discussed in Section 4.3.1.

From the Hα line profile in the spectrum of R81, we can see clear P-Cygni profile. This profile shows that there is a spherical shell of material surrounding the star. Figure 4.3 is the dynamical spectra of the Hα line. In this plot each spectrum is plotted by its phase which is on the left hand side vertical axis. The spectral intensities are plotted in color with values given by the color bar on the right hand side. The continuum is colored purple, while as you go up the color bar is emission and down the color bar is absorption. The top horizontal axis is the wavelength of the spectra. The bottom horizontal axis is the heliocentric velocity of the Hα line. This is calculated from Equation 3.2 where λ_0 is the rest wavelength of Hα (≈ 6562Å). From the dynamical spectra we can see that the Hα line does not change with the phase. This tells us that the material is outside of the system and is in a spherical shell surrounding the system. Also, since there are no double peaks in the Hα line, we know that the material is not rotating, but just expanding outward from the system at approximately 300 km s^{-1}.

4.3 Interpretations

One of the most intriguing things about the data can be seen in the dynamical spectra of Figure 4.3. Looking at the emission of the Hα line over the orbit of this system, we can see a steady increase in the emission until a maximum right before phase $\phi = 0.8$. After this maximum, the emission seems to drop off rather quickly until a slight increase around phase $\phi = 0.08$ where after it begins to decrease again. Comparing the dynamical spectra with the orbit in Figure 3.1, we can try to determine the physical cause of the variability of the Hα emission feature. The following sections contain the theories we tried to describe the observational data with. Some of the orginal models were not able to explain all the features seen, while others are still in the process of testing the validity.

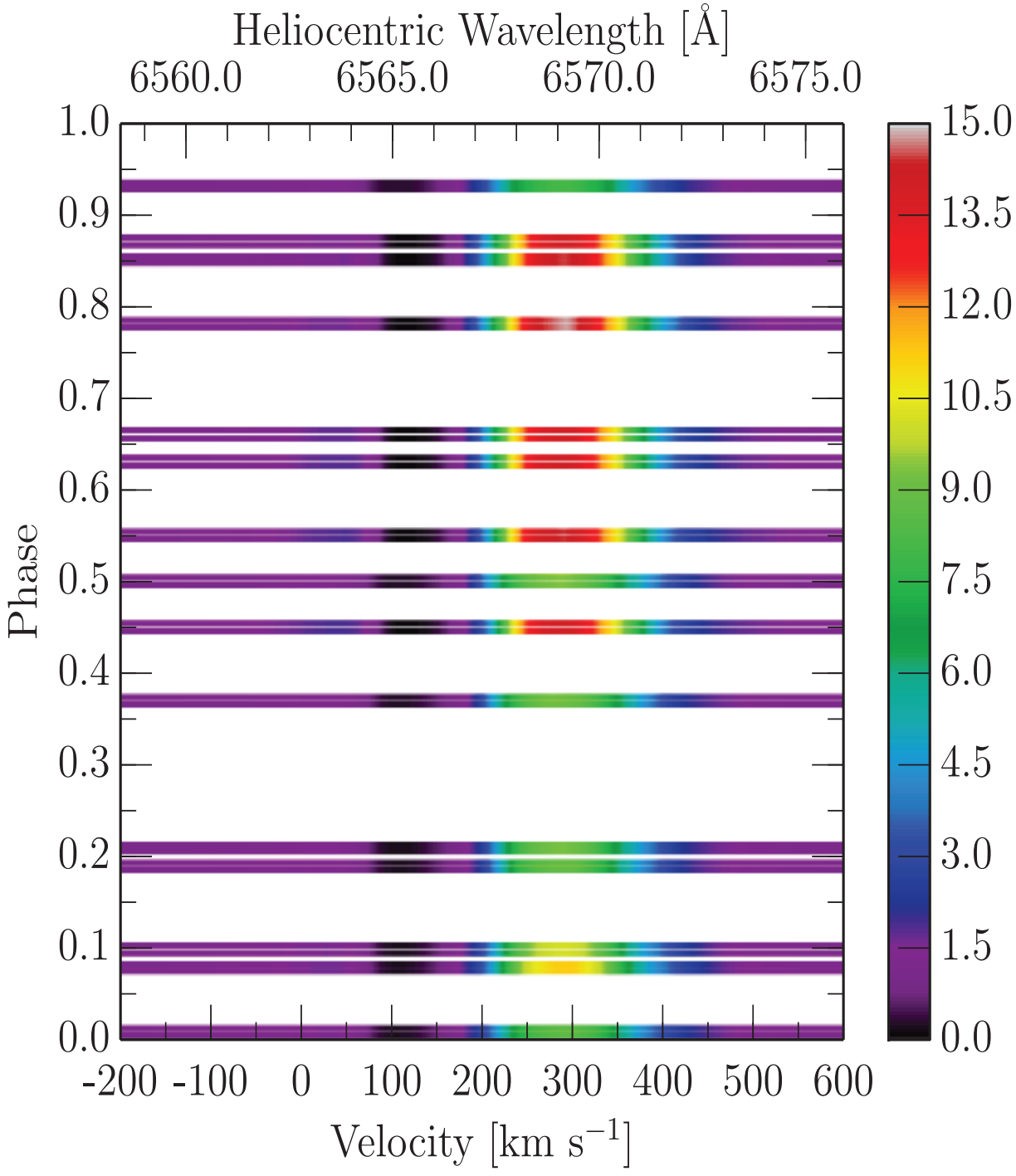

Figure 4.3 Dynamical Spectra of the Hα line in the spectrum of R81.

4.3.1 Mass Transfer Stream

Our first interpretation is that this emission peak is coming from a mass transfer between the two stars. If the primary star is losing mass through a stream to the secondary, this in falling material would become excited and cause an increase in emission. The material would be contained in between the stars and would only be visible when our line of sight falls between the stars. From Figure 3.1, we can see that around phases $\phi = 0.08$ and $\phi = 0.8$ our line of sight falls between the two stars. However, if this is the process that is causing the emission increase we should be seeing a much larger increase around phase $\phi = 0.08$ like that of $\phi = 0.8$. During these phases our line of sight is between the two stars and we would be able to see any mass stream between them. This leads us to concluded that the emission increase is not due to a mass transfer stream in this system.

4.3.2 Interacting Bulge

Due to the eccentric orbit and the relative closeness of these stars, there is a bulge of material on the primary star. This bulge would be caused by the gravitational force from the secondary star and therefore would be in the direction of the secondary. As the two stars approach periastron, the bulge would be closer to the secondary star. Being this close to the secondary star, the gravitational force on the bulge may cause the bulge to feel some tidal friction and depending on the radii of the stars, the bugle may even come into contact with the secondary. Either of these cases could cause the material in the bulge to become excited which would cause an increase in emission. This model fails when looking at the phase location of the emission maximums. If this were a result of an interacting bulge we should be seeing the emission increase earlier around phase $\phi \approx 0.6$ when the bulge would be most visible to us. We do not observe this increase at phase $\phi = 0.6$ in the dynamical spectra and conclude that the emission increase is not due to a bulge on the primary star.

4.3.3 Possible Models and Next Steps

While the original theories were not able to explain the systems observed features there are still some models that are being examined to see if they are able to explain the features of this system. The first explanation is that this emission increase is due to with the intrinsic variability of the primary star. Tubbesing et al. (2002) described the primary star of R81 to be a LBV and therefore would have large variations in its spectra in brightness. If the star is experiencing pulsations in its brightness (this may be the underlying periodicity of the light curve seen in Figure 4.1.b) , this may be driving an increase in it's mass loss rate. This would cause more material to be surrounding the star which would then be excited by the radiation. This would be seen as an increase in emission in the spectra. This would also explain why it seems to only happen at one phase of the orbit, as the star would be undergoing periodic pulsations.

Another possible explanation for this increase is that the physical distance between the primary star and the material surrounding the system is changing during the orbit. As the stars approach apastron, the distance between the primary star and the edge of the outflow material decreases. Since the primary star is closer to the material it can radiate more energy into this material causing the increase in emission. This interpretation explains the lag between when we see the emission and when the stars are aligned with out line of sight. Since it would take some amount of time for the material to become excited, the stars would already be just out of apastron when we begin to observe the increase in the emission.

In order to determine the true process that is taking place in this system these interpretations need to be modeled and tested to see if they can explain all the features that are observed in the data. The next step in this project is to create models of each of these physical situations and see which ones give results similar to the data we observe. These models will be computer based and should allow us to determine what is happening in this system. These models and results are

expected to be published in a article in the *Monthly Notices of the Royal Astronomical Society* in the coming months.

Bibliography

Abt H. A., 1983, ARA&A, 21, 343

Appenzeller I., 1972, PASJ, 24, 483

Carroll, B. and Ostlie, D. (2007). An Introduction to Modern Astrophysics. San Francisco: Pearson Addison-Wesley

Emerson D. (2007). Interpreting Astronomical Spectra. Chichester: John Wiley & Sons

Feast M. W., Thackeray A. D., Wesselink A. J., 1960, MNRAS, 121, 337

Fowles, Grant R. (1989). Introduction to Modern Optics. New York: Dover Publications

Hilditch R. W., (2001), An Introduction to Close Binary Stars, Cambridge: Cambridge University Press

Richardson N. D., Gies D. R., Morrison N. D., Schaefer G., ten Brummelaar T., Monnier J. D., Parks J. R., 2012, ASPC, 465, 160

Tubbesing S., et al., 2002, A&A, 389, 931

Tubbesing S., Kaufer A., Schmid H. M., Stahl O., Wolf B., 2001, ASPC, 233, 163

Wolf B., Stahl O., de Groot M. J. H., Sterken C., 1981, A&A, 103, 427

Vik Dhillon, University of Sheffield

http://www.vikdhillon.staff.shef.ac.uk/seminars/lives_of_ binary_stars/masstrans.html